Microelectrode Array With Integrated Pneumatic Channels for Dynamic Control of Electrode Position in Retinal Implants

Yuanhao Xu and Stella Pang, *Fellow, IEEE*

***Abstract*— Retinal prostheses are biomedical devices that directly utilize electrical stimulation to create an artificial vision to help patients with retinal diseases such as retinitis pigmentosa. A major challenge in the microelectrode array (MEA) design for retinal prosthesis is to have a close topographical fit on the retinal surface. The local retinal topography can cause the electrodes in certain areas to have gaps up to several hundred micrometers from the retinal surface, resulting in impaired, or totally lost electrode functions in specific areas of the MEA. In this manuscript, an MEA with dynamically controlled electrode positions was proposed to reduce the electrode-retina distance and eliminate areas with poor contact after implantation. The MEA prototype had a polydimethylsiloxane and polyimide hybrid flexible substrate with gold interconnect lines and poly(3,4-ethylenedioxythiophene) polystyrene sulfonate electrodes. Ring shaped counter electrodes were placed around the main electrodes to measure the distance between the electrode and the model retinal surface in real time. The results showed that this MEA design could reduce electrode-retina distance up to 100 μm with 200 kPa pressure. Meanwhile, the impedance between the main and counter electrodes increased with smaller electrode-model retinal surface distance. Thus, the change of electrode-counter electrode impedance could be used to measure the separation gap and to confirm successful electrode contact without the need of optical coherence tomography scan. The amplitude of the stimulation signal on the model retinal surface with originally poor contact could be significantly improved after pressure was applied to reduce the gap.**

***Index Terms*— Conductive polymer, microelectrodes, pneumatic actuators, position control, position measurement, prosthetics.**

I. Introduction

RETINAL prostheses are implantable biomedical devices that provide electrical impulses to the retina of individuals with significant retinal diseases to create artificial vision. In normal human eyes, light-sensitive pigments in photoreceptor cells within the outer retinal layer can transduce light stimulation to neural signals. These signals are processed in a complex neural network including the retinal ganglion cells (RGCs) in the inner retinal layer, and eventually transmitted to the visual cortex to form vision. Patients with damaged or degenerated photoreceptor cells induced by physical damage or diseases such as retinitis pigmentosa could not convert light stimuli into neural signals properly, resulting in loss of vision [1], [2]. However, the other structures in the visual system including RGC, optic nerves, and visual cortex may still be intact, thus it is possible to recreate vision by directly applying electrical impulses to the inner retinal layer.

Retinal prosthesis technology has been developing rapidly in the past decades, some products were already put in clinical trials as humanitarian devices, most notably the Argus prosthesis system [3]–[5]. Most of these products consist of three major parts, including a camera to capture the real-time image, a video processing unit to process the images into electrical impulses, and a microelectrode array (MEA) implanted to the retinal surface to stimulate the RGCs. MEA is the only component to have a direct interface with the retina and is crucial to the overall performance of the system. Thus, improving the MEA designs is a major research focus in the retinal prosthesis. A number of studies have been carried out to improve the functionalities of MEA, such as increasing the number of electrodes to enhance resolution [6]–[8], using foldable structures to enhance the coverage of MEA on the retinal surface [9], or using photovoltaic cells powered electrodes to directly replace photoreceptor cells without the need of external cameras [10], [11].

A fundamental limitation of conventional MEA is the lack of conformity to contact the retinal layers in both epiretinal and subretinal implants. The electric field becomes more divergent in the RGC region with larger electrode-retina distance. Although MEA could be pre-curved to enhance the contact, some electrodes may still have relatively large gaps up to several hundred micrometers from the retinal surface due to the variation of localized retinal topography of individuals [12], [13]. As a result, specific regions on MEA could suffer from poor signal quality, or even complete loss of signal. Currently, most retina MEAs used *in-vivo* still have relatively rigid substrates to successfully implant the MEA to the designated layer from a small incision on the eyeball. Ultra-flexible MEA with dissolvable substrates has been tested

Manuscript received August 12, 2021; revised October 5, 2021; accepted October 24, 2021. Date of publication October 27, 2021; date of current version November 9, 2021. This work was supported in part by the Center for Biosystems, Neuroscience, and Nanotechnology (CBNN), City University of Hong Kong, under Grant 9360148, and Grant 9380062; and in part by the University Grants Council of Hong Kong, through the General Research Fund (GRF) under Project 11218017, Project 11213018, Project 11212519, and Project 11207620. *(Corresponding author: Stella Pang.)*

The authors are with the Electrical Engineering Department, City University of Hong Kong, Hong Kong, China (e-mail: yuanhaoxu2@cityu.edu.hk; pang@cityu.edu.hk).

This article has supplementary downloadable material available at https://doi.org/10.1109/TNSRE.2021.3123754, provided by the authors.

Digital Object Identifier 10.1109/TNSRE.2021.3123754

in other applications [14]. Although the ultra-flexible design could better fit the surface topographies, it was still a challenge to naturally fill small gaps and sharp corners with a planar device, resulting in relatively poor contact in some regions. External forces would be needed in such situations to physically deform the substrate and fill these small gaps. Some studies used needle-shaped electrodes to physically poke into the retina layers, which would enhance the signal but potentially damage the retina [15].

Another problem is the lack of real-time monitoring and adjustment of electrode-retina gap after MEA insertion. Conventionally, optical coherence tomography (OCT) scan is needed to observe the contact of MEA with the retinal surface. Related studies also showed that electrode impedance in the MEA changed with electrode-retina distance, thus it could be used as an alternative indicator of contact quality [16]–[18]. However, these studies did not have a position control feature for individual electrodes, and an additional surgical operation may be needed if the contact is not good enough, which can be both time-consuming, costly and dangerous.

Thus, prototype of a new MEA design with real-time control of electrode position and monitoring of electrode-model retinal surface distance was proposed in this work. Pneumatic cavities were placed underneath the electrodes to dynamically adjust the electrode positions by changing the pneumatic pressure. Ring shaped counter electrodes were placed around the main electrodes to measure the electrode-model retinal surface distance in real time. The MEA substrate was fabricated in polydimethylsiloxane (PDMS) with cavities that could be inflated under pneumatic pressure to reduce the distance between the targeted surface and PDMS membrane with an initial gap. Conductive polymer poly(3,4-ethylenedioxythiophene) polystyrene sulfonate (PEDOT:PSS) was used as the electrode material to facilitate the high stretching capability of the PDMS substrate, while gold (Au) was used for the interconnect wires to reduce the impedance.

II. Materials and Methods

A. Microfabrication Technology

MEA with polyimide (PI) substrate, PDMS microchannels/microcavities, Au/Cr interconnect lines, and PEDOT:PSS electrodes were fabricated using microfabrication techniques. Silicon (Si) stamps of PDMS microchannels/microcavities were fabricated by multiple switching cycles of deep reactive ion etching (DRIE) process. The DRIE Bosch process was carried out by switching of 7 s passivation cycle with 85 sccm C_4F_8, 600 W coil power at 20 mTorr, and 14 s etch cycle with 130 sccm SF_6, 600 W coil power, 20 W platen power at 40 mTorr to etch the deep trenches. 68 and 34 alternative cycles were applied to fabricate Si stamps that would be replicated into 100 μm high microchannels and 50 μm thick PDMS membranes, respectively. The Si stamp was first coated with 4:1 methacryl oxypropylene trichlorosilane (MOPTS) trichloro (1H, 1H, 2H, 2H-perfluorooctyl) silane (FOTS) to adjust the surface energy as shown in Fig. 1(a). PDMS prepolymer (10:1 silicone elastomer base curing agent, Dow corning Sylgard 184) was casted on the Si stamp and imprinted on a flat Si wafer coated with FOTS, then cured for overnight

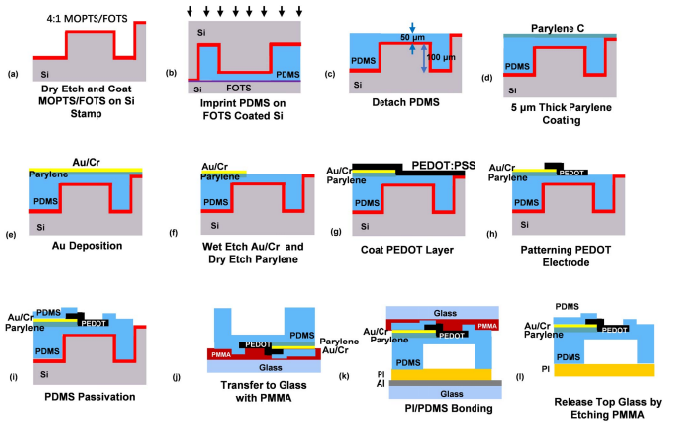

Fig. 1. Fabrication technology of retinal microelectrode array (MEA). (a-c) PDMS microchannels were imprinted with Si stamp. (d-f) Au/Cr interconnects were patterned on PDMS microchannels with Parylene C intermediate layer to improve adhesion and prevent cracks. (g-i) PEDOT:PSS electrodes were patterned to provide electrode stretching capability. (j-l) PDMS channels were bonded to PI substrates with PMMA and Al sacrificial layers.

as shown in Fig. 1(b). After detaching, cured PDMS stayed on the Si stamp due to its higher surface energy as shown in Fig. 1(c).

A 3 μm thick parylene C layer was deposited on PDMS as an intermediate layer to enhance adhesion and prevent cracks on metal interconnect lines, as shown in Fig. 1(d). 100/10 nm thick Au/Cr layer was deposited on parylene C by thermal evaporation as shown in Fig. 1(e). The interconnect lines were patterned by photolithography, followed by wet etching of Au/Cr layers and O_2 plasma etching of parylene C layer with 10 sccm O_2 at 10 mTorr pressure and 450 W power for 5 min, as shown in Fig 1(f). A PEDOT:PSS solution was spin-coated and baked at 110 °C for 15 min as shown in Fig. 1(g). The 300 nm thick PEDOT:PSS electrodes were patterned by photolithography and O_2 plasma etching as shown in Fig. 1(h). A 1 μm thick PDMS passivation layer was spin coated on top of the electrodes and interconnect lines, and the electrodes and connecting pads were opened by dry etching in 35 sccm SF_6, 16 sccm CF_4, 16 sccm O_2 with 15 mTorr pressure and 1500 W power for 2 min as shown in Fig. 1(i).

The PDMS microchannels/microcavities with the interconnect lines and electrodes were transferred to a glass slide using poly(methyl methacrylate) (PMMA) as an intermediate layer, as shown in Fig 1(j). The PDMS structure was chemically bonded to a PI substrate with a monolayer of (3-mercaptopropyl)trimethoxysilane and (3-glycidyloxypropyl)trimethoxysilane coating on PDMS and PI surface, respectively, as shown in Fig. 1(k). PMMA and Al sacrificial layers were then removed to release the MEA from the top and bottom glass slides as shown in Fig 1(l).

B. Assembly of MEA

Layered schematic of the MEA is shown in Fig. 2(a). Shank of the MEA was 1 mm wide and 10 mm long. Three electrode pairs were placed with center to center separation of 1 mm. Each electrode pair consisted of a main electrode of 150 μm diameter (dia.) and a ring-shaped counter electrode of 200 μm inner dia. and 300 μm outer dia. These parameters

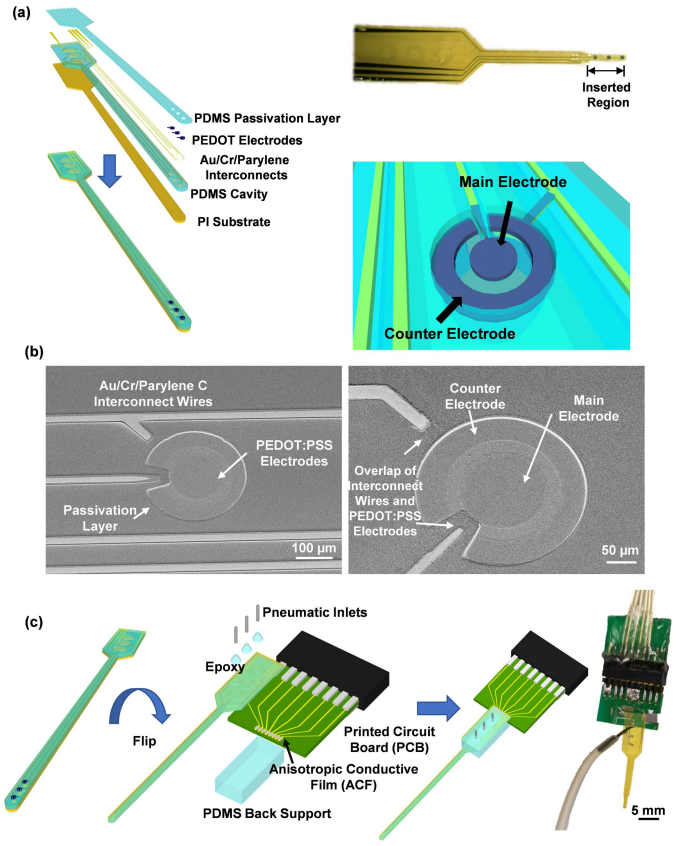

Fig. 2. Schematic and micrographs of retinal MEA. (a) Detailed layers and micrographs of MEA. Electrode region would be inserted into eyeball. (b) PEDOT:PSS electrode and Au/Cr interconnects. Metal-PEDOT overlapping area ensured good connectivity between electrodes and interconnect wires. Ring-shaped counter electrode was placed around main electrode to measure real-time electrode-retina distance. (c) Schematics and micrographs of MEA assembled on PCB board. Au/Cr contact pads were connected to PCB board via ACF tapes. Steel pneumatic inlets were fixed and sealed by epoxy. PDMS back support was applied to enhance stability.

were designed according to the size of rats with eye dia. of ~6 mm. The other end of the MEA had 3 inlets to control the displacement of electrodes independently. 4 connecting pads (3 for each main electrode, 1 for all counter electrodes) were connected to a printed circuit board (PCB) for testing. An overlapping area of PEDOT:PSS electrodes and Au/Cr interconnect lines were designed to enhance electrical conductivity as shown in Fig. 2(b).

Packaging of MEA is shown in Fig. 2(c). Stainless steel needles were inserted to pneumatic inlets to connect the microchannels and microcavities to syringes to apply pneumatic pressure. Epoxy was added around the connecting parts to prevent leakage. Connecting pads of the MEA were aligned and bonded to the connection pins on PCB via anisotropic conductive film (ACF) tape. A bulk PDMS block was bonded to the backside as supporting structure to sandwich the PCB in the middle to enhance structural stability.

C. Numerical Simulation

Numerical simulation of PDMS membrane displacement and electrical properties of the microelectrodes were performed on COMSOL Multiphysics commercial software. A 2-step simulation was performed to evaluate the electrical performance of the electrode pairs under membrane displacement. In step one, a solid mechanics module was applied to investigate the expansion of the PDMS cavity with applied pneumatic pressure, in which PDMS was set as nearly incompressible hyperelastic material with Neo-Hookean model. The shear and bulk modulus of PDMS was selected based on a previous study [19]. In step two, the exported geometric changes from step one was used to simulate the electric field distribution and main-counter electrode impedance with various initial electrode-model retinal gaps. Kasi's retina model was used in this simulation [20], [21], which included bulk fluid with conductivity of 2 S/m and relative permittivity of 78.5, and a changing conductivity across the retinal layers.

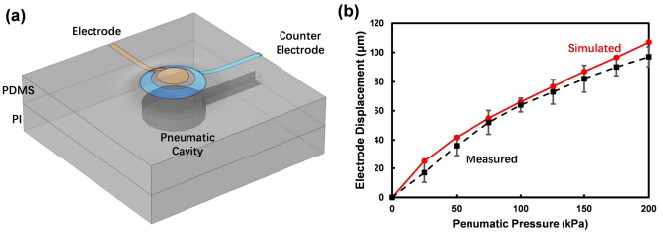

Fig. 3. Electrode displacement increased with pneumatic pressure. (a) Numerical simulation setup. PDMS membrane expanded with applied pneumatic pressure. PI substrate did not have significant deformation due to large Young's modulus. (b) Comparison of simulation and measured electrode displacement. Electrode displacement increased with increasing pneumatic pressure in microchannels. Simulation and measured results matched well.

D. Electrode Displacement Measurement

Diluted celltrace calcein green AM (Invitrogen) was patterned on the surface of the electrodes. Fluorescent micrographs of the MEA were imaged by Nikon Eclipse NI-U upright microscope to find the focus plane before and after PDMS cavity expansion. Electrode displacement was calculated by the change of z-plane.

E. Electrical Measurement and Data Analysis

Impedance of the electrodes was measured by Reference 600+ Potentiostats (Gamry Instruments, Warminster, US). Measurement results shown in this work were obtained using an input voltage of 10 mV at 10^4 Hz frequency.

All measured data was shown in average value with standard deviation. Data were compared by Student's t-test. A p-value smaller than 0.05 indicates significant statistical difference.

III. Experimental Results

A. Electrode Displacement Increased With Pneumatic Pressure

Due to the high elasticity of PDMS, the microcavity underneath an electrode expanded when pneumatic pressure was applied as shown in Fig. 3(a). Electrodes had significant displacement in the vertical direction, and the electrode displacement became larger when higher pneumatic pressure was applied. With 400 μm dia., 100 μm high cavity and 50 μm thick membrane, the electrode on top had vertical displacement up to 100 μm with 200 kPa pneumatic pressure. Changes in electrode displacement with increasing pneumatic pressure are

shown in Fig. 3(b). The simulation and measurement results matched well. No significant expansion on PI substrate was observed in simulation or measurement.

With high pneumatic pressure and large vertical electrode displacement, the electrode also underwent extensive stretching. With 200 kPa pressure, the elongation ratio of PDMS membrane reached 25%, which was far beyond the stretching limit of most metals. If Au electrodes were used, they would have severe cracks. Instead, PEDOT:PSS electrodes could be stretched up to 30% without cracking, making it the better electrode material under this circumstance [22], [23]. In this MEA design, the inflated regions consisted of PEDOT:PSS as the conducting material to avoid cracks, while other regions had Au layers to ensure the overall conductivity. The comparison of the probe performance with Au and PEDOT:PSS electrodes are shown in supplementary Fig. S1. Au electrodes cracked and wrinkled severely after 10 % membrane stretching, resulting in significantly increased impedance. Meanwhile, PEDOT:PSS electrodes only had minimal wrinkles on the surface after stretching, and the impedance was stable with pressure applied up to 250 kPa. The device was tested in cyclic loads of 250 kPa pressure with a stable performance.

B. Increased Main-Counter Electrode Impedance With Smaller Electrode-Model Retina Gap

Ring-shaped electrode designs have been widely used in retinal stimulation. In most cases, the outer ring electrode served as a local return to confine the activated RGC region of the center electrode [24], [25]. Some studies also showed that a group of ring-shaped electrodes could be used to produce virtual electrodes to enhance visual acuity [26]. The electrode pair design in this work had multiple functions as shown in Fig. 4(a). In normal working mode where electrical impulses were sent to stimulate RGC, the ring-shaped counter electrodes were grounded, and could enhance overall performance by reducing crosstalk of adjacent main electrodes. More importantly, the electrode pairs could be used to measure the gap between the electrode and the retinal surface, in which case the ring-shaped electrode was used as a counter electrode to measure the impedance with the main electrode. When electrodes had poor contact with the retinal surface, bulk fluid filled in the gaps. Since bulk fluid was rich of ions such as Na^+ and K^+, the conductivity was relatively high, whereas the retina itself had significantly lower conductivity. Thus, the impedance was different among the scenarios when the electrode and the retinal surface had direct contact, in close proximity, or far away from each other.

Numerical simulation was performed to validate the distance measurement feature. Initial retina-electrode gap of 100 μm with zero pressure was used. A 2-step simulation setup is shown in Fig. 4(b). Geometric deformation of the PDMS membrane under specific pneumatic pressure was simulated in step 1. Electric potential distribution and main-counter electrode impedance were simulated in step 2 using the exported geometry with reduced distance from the previous step. The simulation results followed the expected trend as shown in Fig. 4(c). When the pneumatic pressure increased, the PDMS membrane expanded accordingly, and the electrode-model retinal surface distance was reduced. Simulated electrode-

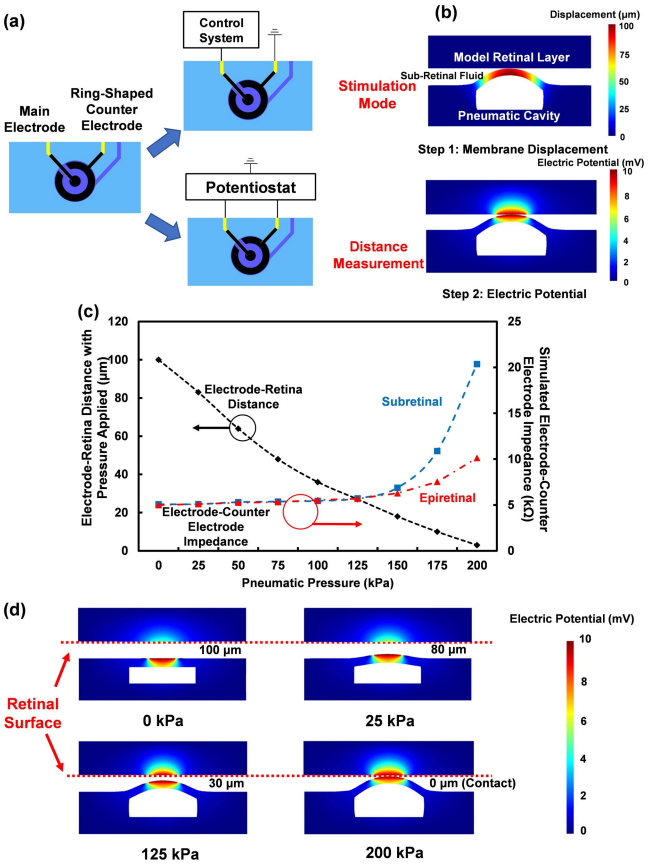

Fig. 4. Design and simulation of electrode-model retina distance. (a) Paired electrode design to measure real-time electrode-model retina distance. In distance measurement mode, ring-shaped counter electrode was utilized to obtain impedance to determine electrode-retina distance; in stimulation mode, counter electrode was grounded to shield interference between adjacent main electrodes. (b) Two-step simulation of impedance and distance with 100 μm initial gap and 10 mV, 10^4 Hz power input in distance-measurement mode. Electrode-model retina distance was calculated with applied pneumatic pressure. Impedance between main and counter electrode was simulated with corresponding electrode-model retina distance. (c) Simulated impedance between main and counter electrode increased with decreasing electrode-retinal gap due to applied pressure. (d) Electric potential distribution with various electrode-model retinal gaps. Electrical signal was large enough to stimulate retinal cells while in close proximity.

counter electrode impedance increased with increased pressure and decreased electrode-model retina distance, the change became more noticeable when the distance was smaller than 20 μm. In the subretinal model, with zero pneumatic pressure, main-counter electrode impedance was low at 5.2 kΩ. When pneumatic pressure increased to 150 kPa, electrode-retina distance was reduced to 20 μm as shown in Fig. 4(c), while impedance slowly increased to 6.9 kΩ during the process. With further increased pressure to 200 kPa, electrode made direct contact with the model retinal surface, and the impedance drastically increased to 20.4 kΩ. On the other hand, the impedance changes in epiretinal implant model were smaller compared to the subretinal model. However, the impedance changes were still noticeable and could be used to indicate the separation between the electrodes and the retinal layer.

It was noticed that electrical impulses could better stimulate the retinal layer with electrode-retina gap smaller than 30 μm, as indicated by increased electric potential on the model retinal surface as shown in Fig. 4(d). Thus, the feedback from

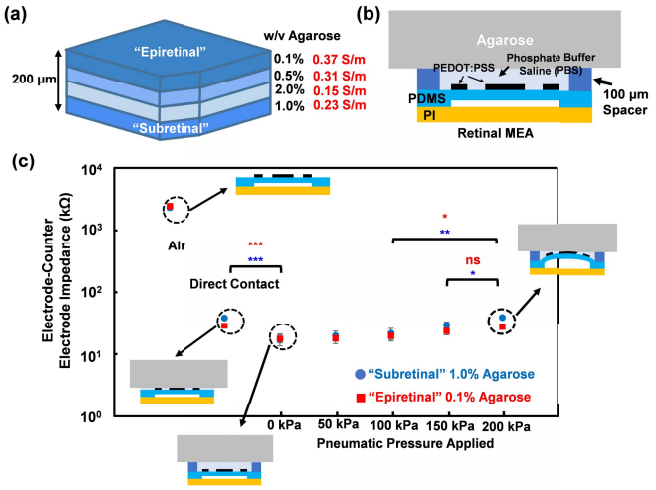

Fig. 5. *In-vitro* testing of the pneumatically controlled MEA. (a) Schematic of agarose model retina mimicking Kasi's retina model. Electrical conductivity in various layers was different due to changing agarose concentration from 0.1 to 2.0% w/v. Conductivity profile was similar to rat retina. Model retina was 1 × 1 cm^2 in size, and one corner was cut to mark the orientation. (b) Test platform setup. PBS and agarose sheet represented the sub-retinal fluid and retina layer, respectively. Spacer was added to provide initial gap of 100 μm. (c) Measurement results on testing platform. MEA in air without PBS and MEA directly contacting agarose sheet without spacer were used as control groups. Main electrode-counter electrode impedance increased with increased pneumatic pressure. P value was derived by Student's t-test with *p <0.05, **p <0.01, ***p <0.001, and ns for not significant.

main-counter electrode impedance served as a good indicator of whether the electrode was in close proximity to the retinal surface in order to provide effective stimulation. It should be clarified that the simulations were carried out in the smaller region around the electrodes, the effects of interconnect lines and possible input impedance from various junctions were not taken into consideration, thus the measured impedance was larger than the simulated one.

C. In-Vitro Testing of MEA Distance Measurement Module

PBS was used as the bulk fluid and a 200 μm thick agarose membrane with multiple layers was used to mimic the model retina in this *in-vitro* experiment. The structure of the agarose sheet was shown in Fig. 5(a), where the front and backside of the sheet resembled the epiretinal and subretinal layers, respectively. 100 μm thick PDMS spacer was placed between the MEA and the agarose sheet to provide the initial gap. The whole platform was submerged in PBS to fill the gap as shown in Fig. 5(b). Pneumatic pressure was applied to the PDMS cavity and the impedance between the main and counter electrodes was measured. Two control groups were added. MEA in control group 1 was tested in air without any extra element, while MEA in control group 2 was submerged in PBS, but was directly in contact with the agarose sheet to mimic the condition with direct electrode-retina contact. Both epiretinal and subretinal models were measured using frontside and backside of the agarose model retina. Experiments were repeated 3 times with 3 different devices. Average impedance under various conditions with error bar is shown in Fig. 5(c).

The impedance of interconnect lines and contact pads were measured by directly placing platinum probes at the two terminals using micropositioners, the average measured value was 976±58 Ω. When the MEAs were submerged in PBS and under zero pneumatic pressure with the 100 μm gap, the measured impedance was 17.5 and 17.2 kΩ for epiretinal and subretinal models, respectively. Lower conductivity of PEDOT:PSS and electrical double layer effect at electrode and PBS interface contributed to these impedances. Impedance increased with increasing pneumatic pressure. Like the simulation results, the measured impedance changes were not significant until pneumatic pressure reached 100 kPa and above. With 200 kPa pressure, the impedance raised to 27.3 and 39.2 kΩ for epiretinal and subretinal models, respectively. This result was almost identical to the value measured in control group 2, where the electrode and the agarose sheet had direct contact. These experimental results proved that the distance measurement module could provide real time feedback of successful electrode-retina contact.

D. In-Vitro Testing of MEA Performance With Complex Retina Topography

Due to complex topography of retinal surface, initial gaps between individual electrodes and retinal surface could be different. To test the performance of MEA under such circumstance, 20, 60, and 100 μm thick PDMS spacers were placed around 3 individual electrodes on the MEA to create different initial electrode-model retinal gaps. Three micropositioners were used to place platinum probes to the agarose model retina surfaces. The probes were connected to an oscilloscope to measure the signal strength. The MEA was connected to a frequency generator and a potentiostat. During distance measurement, the potentiostat was switched on to measure main electrode-counter electrode impedance of the 3 electrode pairs. During stimulation, the function generator was switched on to provide 10 mV, 10^4 Hz signal to the 3 main electrodes, and the counter electrodes were grounded. The schematic of the testing platform is shown in Fig. 6(a).

When the input signal was the same, signal strength on the model retinal surface was directly determined by the distance between the electrode and the model retinal surface. Electric potential on the model retinal surface was identical to the MEA input signal with direct contact; signal strength on the model retinal surface decreased with increasing electrode-retina distance as shown in Fig. 6(b). The electric potential measured on the model retinal surface with 10 mV input voltage and 20, 60, and 100 μm gaps were 8.7, 5.5, and 3.4 mV, respectively, with electrodes of 150 μm dia. If the MEA did not have any electrode position control features, the input signal need to be increased for compensation. When smaller electrodes with 30 and 50 μm dia. were used, the initial electric potential measured became even weaker.

To enhance the performance, pneumatic pressure was applied within the PDMS cavity to decrease electrode-model retina gaps. Before pressure was applied, a range of main-counter electrode impedance for successful electrode-retina contact was derived by measuring the impedance with direct electrode-model retina contact. As pneumatic pressure in the PDMS cavities was gradually increased, the main-counter electrode impedance was measured continuously. Once the impedance reached the designated range, the pneumatic

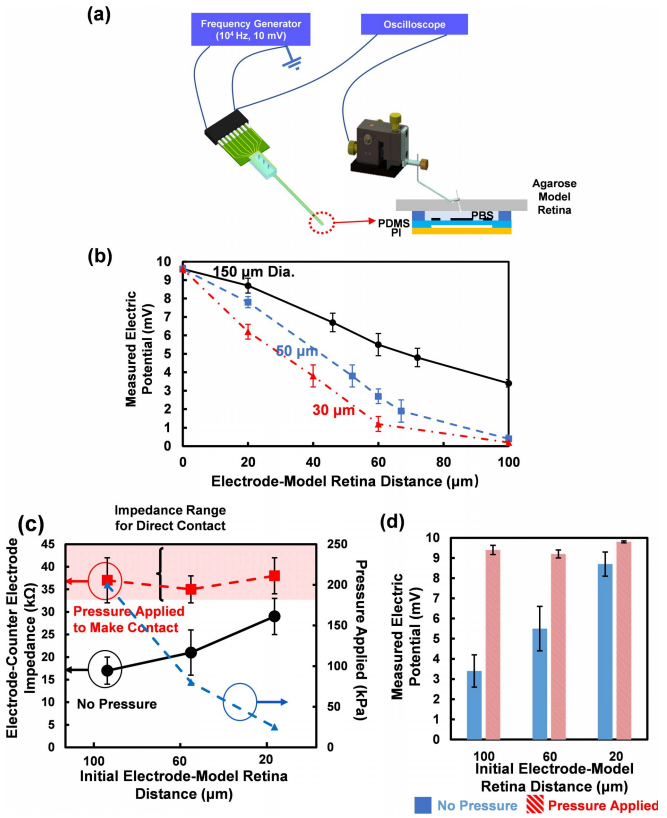

Fig. 6. *In-vitro* characterization of electric potential at designated electrode contact surface with various initial electrode-model retina distance. (a) Schematic of *in-vitro* measurement setup. MEA was connected to frequency generator to provide 10 mV at 10^4 Hz at main electrode. Initial electrode-model retina gap was created by PDMS spacer with 20, 60, and 100 μm thickness. Electric potential at agarose surface was measured using oscilloscope via platinum probe controlled by micro-positioner. (b) Measured electric potential decreased with increasing gap between electrodes and model retinal surface. (c) Comparison of electrode-counter electrode impedance before and after pressure applied. All 3 electrodes could be controlled to enter designated range of successful electrode-retina contact using different applied pressure. (d) Comparison of electric potential on model retinal surface before and after pressure was applied. Performance was significantly enhanced for all 3 electrodes with applied pressure.

pressure was fixed. The comparison of the main-counter electrode impedance before and after pressure was applied is shown in Fig. 6(c). The pressure needed for electrodes to reach the designated range for successful contact was 200, 80 and 30 kPa with 100, 60 and 20 μm gaps, respectively.

Electric potential on the model retinal surface before and after applying the pressure is shown in Fig. 6(d). The received signal on the model retinal surface above the 3 electrodes was significantly different before pressure was applied. After providing the proper pressure, the received signal strength was improved, and the signal variation no longer existed. It is worth to note that no monitoring using a microscope was needed during the electrode position control, and the feedback of the electrode position was purely based on measurement of main-counter electrode impedance.

IV. Discussion

PDMS based pneumatic actuators have been widely used in biomedical applications such as microfluidic valves [27]–[29]. The biocompatibility and stretching capability of this material made it a good candidate for implant devices that required material shape manipulation. In this work, a PDMS based retinal MEA prototype was developed that could reduce electrode-retina gap by pneumatically controlled expansion of the PDMS membrane, and the main-counter electrode pairs could be used to measure the electrode-model retina distance in real-time without tomography. The results showed that this MEA device could successfully reduce the electrode-model retina gap up to 100 μm. The enhanced electrode-model retinal contact could provide a more convergent electric field in the RGC region, which could greatly enhance the signal strength and remove the large variation of signal amplitude due to complex topography on the retinal surface.

The non-homogenous contact will always be a problem for retinal MEA due to complex retinal topography, and motion or vibration in daily activities of patients. Currently, the majority of MEA used in animal test and clinical trials had relatively large electrodes ranging from 30-200 μm dia., which overshadowed this problem [5], [16], [30]–[32]. With large electrode area, the input signal amplitude could be increased in regions with poor contact to compensate the signal reduction due to large electrode-retina gaps. However, to achieve higher signal resolution, it is necessary to have electrodes with smaller sizes, and the effect of poor electrode-retina contact will become increasingly obvious [33], [34]. Thus, the electrode position control feature will be essential in future MEA designs. Pneumatic or hydraulic actuation of flexible membrane is a mechanical method for micro-position control. Thus, it would not introduce electrical interference to the electrodes comparing to other methods such as electrostatic or electromagnetic actuation. The pneumatic or hydraulic inlet channels could also be implemented in parallel with the interconnect lines of electrodes. The inlet could be placed on the PCB board, which makes this design compatible with the majority of conventional retinal MEA. The stretching of electrode on elastic membrane could cause cracks on gold or platinum electrodes. This problem could be solved by using conductive polymer as the electrode material, which could provide a relatively stable electrode impedance at low strain. Hence the combination of pressure actuated flexible membrane and electrodes fabricated by conductive polymer such as PEDOT:PSS is a good candidate for electrode position control in retinal implants. Conventionally, OCT scan is needed to check the contact between electrodes and the retinal surface. The MEA device presented in this paper used an impedance-based method to measure the electrode-retinal distance, which could provide fast feedback and would be more suitable for routine adjustment in daily use. It is worth to note that since normal human eyes have intraocular pressure of 1.8-2 kPa with daily variations [35], a higher actuation pressure in *in-vivo* applications is preferred to reduce its effect on the stability of the pneumatically controlled device. Using pressurized devices *in-vivo* can bring potential risk to the implanted region. The effects in retinal implants would need further evaluation.

The MEA demonstrated in this work was a prototype with 3 electrode pairs and 3 pneumatic cavities, where the position of each electrode pairs was controlled separately. Most state-of-the-art retinal MEA were implemented with hundreds of electrodes, to facilitate each of them with individual cavities would be complicated. A possible solution will be to

separate the electrodes into groups, and control each group of electrodes with a single cavity. The impedance-based electrode-retina distance measurement feature was more sensitive with smaller gaps. Although pressure could be gradually enhanced until the impedance feedback indicated a good contact, it is more practical to determine the initial electrode-retinal distance with OCT scan after implant surgery, and use the distance measurement feature to facilitate routine adjustment in daily life. PDMS is known to be permeable to gases including O_2, N_2, and CO_2. Thus in future applications, PDMS needs to have additional treatment to be completely air-tight [36]. An alternative solution is to use hydraulic pressure for membrane actuation, which would provide better long-term stability. The electrode-retinal conformity could be monitored on a regular basis using the impedance-based distance measurement feature, and the pressure could be adjusted as needed. Overall, the electrode position control solution proposed in this work could fill the missing link in retinal MEA applications, and might provide insight for future improvement of retinal prosthesis.

REFERENCES

[1] C. Gargini, E. Terzibasi, F. Mazzoni, and E. Strettoi, "Retinal organization in the retinal degeneration 10 (rd10) mutant mouse: A morphological and ERG study," *J. Comparative Neurol.*, vol. 500, no. 2, pp. 222–238, Jan. 2007.

[2] A. Santos *et al.*, "Preservation of the inner retina in retinitis pigmentosa: A morphometric analysis," *Arch. Ophthalmol.*, vol. 115, no. 4, pp. 511–515, 1997.

[3] A. Ahuja *et al.*, "Blind subjects implanted with the Argus II retinal prosthesis are able to improve performance in a spatial-motor task," *Brit. J. Ophthalmol.*, vol. 95, no. 4, pp. 539–543, 2011.

[4] L. da Cruz *et al.*, "Five-year safety and performance results from the Argus II retinal prosthesis system clinical trial," *Ophthalmology*, vol. 123, no. 10, pp. 2248–2254, Oct. 2016.

[5] J. D. Dorn *et al.*, "The detection of motion by blind subjects with the epiretinal 60-electrode (Argus II) retinal prosthesis," *JAMA Ophthalmol.*, vol. 131, no. 2, pp. 183–189, Feb. 2013.

[6] D. Palanker, A. Vankov, P. Huie, and S. Baccus, "Design of a high-resolution optoelectronic retinal prosthesis," *J. Neural Eng.*, vol. 2, no. 1, pp. S105–S120, Mar. 2005.

[7] S. Nirenberg and C. Pandarinath, "Retinal prosthetic strategy with the capacity to restore normal vision," *Proc. Nat. Acad. Sci. USA*, vol. 109, no. 37, pp. 15012–15017, 2012.

[8] W. Tong, H. Meffin, D. J. Garrett, and M. R. Ibbotson, "Stimulation strategies for improving the resolution of retinal prostheses," *Frontiers Neurosci.*, vol. 14, p. 262, Mar. 2020.

[9] H. Ameri, T. Ratanapakorn, S. Ufer, H. Eckhardt, M. S. Humayun, and J. D. Weiland, "Toward a wide-field retinal prosthesis," *J. Neural Eng.*, vol. 6, no. 3, Jun. 2009, Art. no. 035002.

[10] K. Mathieson *et al.*, "Photovoltaic retinal prosthesis with high pixel density," *Nature Photon.*, vol. 6, no. 6, pp. 391–397, 2012.

[11] J. F. Maya-Vetencourt *et al.*, "A fully organic retinal prosthesis restores vision in a rat model of degenerative blindness," *Nature Mater.*, vol. 16, no. 6, pp. 681–689, Jun. 2017.

[12] M. Velikay-Parel, D. Ivastinovic, T. Georgi, G. Richard, and R. Hornig, "A test method for quantification of stimulus-induced depression effects on perceptual threshold in epiretinal prosthesis," *Acta Ophthalmol.*, vol. 91, no. 8, pp. e595–e602, 2013.

[13] C. J. Abbott *et al.*, "Safety studies for a 44-channel suprachoroidal retinal prosthesis: A chronic passive study," *Investigative Ophthalmol. Vis. Sci.*, vol. 59, no. 3, pp. 1410–1424, 2018.

[14] D.-H. Kim *et al.*, "Dissolvable films of silk fibroin for ultrathin conformal bio-integrated electronics," *Nature Mater.*, vol. 9, no. 6, pp. 511–517, Apr. 2010.

[15] M. E. M. Stamp, W. Tong, K. Ganesan, S. Prawer, M. R. Ibbotson, and D. J. Garrett, "3D diamond electrode array for high-acuity stimulation in neural tissue," *ACS Appl. Bio Mater.*, vol. 3, no. 3, pp. 1544–1552, Mar. 2020, doi: 10.1021/acsabm.9b01165.

[16] M. Mahadevappa, J. D. Weiland, D. Yanai, I. Fine, R. J. Greenberg, and M. S. Humayun, "Perceptual thresholds and electrode impedance in three retinal prosthesis subjects," *IEEE Trans. Neural Syst. Rehabil. Eng.*, vol. 13, no. 2, pp. 201–206, Jun. 2005.

[17] A. Ray, L. L.-H. Chan, A. Gonzalez, M. S. Humayun, and J. D. Weiland, "Impedance as a method to sense proximity at the electrode-retina interface," *IEEE Trans. Neural Syst. Rehabil. Eng.*, vol. 19, no. 6, pp. 696–699, Dec. 2011.

[18] P. Pham, S. Roux, F. Matonti, F. Dupont, V. Agache, and F. Chavane, "Post-implantation impedance spectroscopy of subretinal micro-electrode arrays, OCT imaging and numerical simulation: Towards a more precise neuroprosthesis monitoring tool," *J. Neural Eng.*, vol. 10, no. 4, Aug. 2013, Art. no. 046002.

[19] I. D. Johnston, D. K. McCluskey, C. K. L. Tan, and M. C. Tracey, "Mechanical characterization of bulk Sylgard 184 for microfluidics and microengineering," *J. Micromech. Microeng.*, vol. 24, no. 3, 2014, Art. no. 035017.

[20] H. Kasi, W. Hasenkamp, G. Cosendai, A. Bertsch, and P. Renaud, "Simulation of epiretinal prostheses-evaluation of geometrical factors affecting stimulation thresholds," *J. Neuroeng. Rehabil.*, vol. 8, no. 1, p. 44, 2011.

[21] H. Kasi, R. Meissner, A. Babalian, H. V. Lintel, A. Bertsch, and P. Renaud, "Direct localised measurement of electrical resistivity profile in rat and embryonic chick retinas using a microprobe," *J. Electr. Bioimpedance*, vol. 1, no. 1, pp. 84–92, Dec. 2010.

[22] D. J. Lipomi, J. A. Lee, M. Vosgueritchian, B. C.-K. Tee, J. A. Bolander, and Z. Bao, "Electronic properties of transparent conductive films of PEDOT: PSS on stretchable substrates," *Chem. Mater.*, vol. 24, pp. 373–382, Dec. 2012.

[23] A. Takei, S. Tsukamoto, Y. Komazaki, Y. Kusaka, K. Kuribara, and M. Yoshida, "Stretchable and durable parylene/PEDOT: PSS/parylene multi-layer induced by plastic deformation for stretchable device using functionalized PDMS," *AIP Adv.*, vol. 10, no. 2, 2020, Art. no. 025205.

[24] W. Tong *et al.*, "Improved visual acuity using a retinal implant and an optimized stimulation strategy," *J. Neural Eng.*, vol. 17, no. 1, Dec. 2019, Art. no. 016018.

[25] V. H. Fan *et al.*, "Epiretinal stimulation with local returns enhances selectivity at cellular resolution," *J. Neural Eng.*, vol. 16, no. 2, Apr. 2019, Art. no. 025001.

[26] Q. Lyu *et al.*, "A three-dimensional microelectrode array to generate virtual electrodes for epiretinal prosthesis based on a modeling study," *Int. J. Neural Syst.*, vol. 30, no. 3, Mar. 2020, Art. no. 2050006.

[27] W. Zhang *et al.*, "PMMA/PDMS valves and pumps for disposable microfluidics," *Lab a Chip*, vol. 9, no. 21, pp. 3088–3094, 2009.

[28] T. Pan, S. J. McDonald, E. M. Kai, and B. Ziaie, "A magnetically driven PDMS micropump with ball check-valves," *J. Micromech. Microeng.*, vol. 15, no. 5, p. 1021, 2005.

[29] I. E. Araci and S. R. Quake, "Microfluidic very large scale integration (mVLSI) with integrated micromechanical valves," *Lab Chip*, vol. 12, no. 16, pp. 2803–2806, 2012.

[30] R. Wilke *et al.*, "Spatial resolution and perception of patterns mediated by a subretinal 16-electrode array in patients blinded by hereditary retinal dystrophies," *Invest. Ophthalmol. Vis. Sci.*, vol. 52, no. 8, pp. 5995–6003, Jul. 2011.

[31] R. Samba, T. Herrmann, and G. Zeck, "PEDOT–CNT coated electrodes stimulate retinal neurons at low voltage amplitudes and low charge densities," *J. Neural Eng.*, vol. 12, no. 1, 2015, Art. no. 016014.

[32] C. G. Eleftheriou, J. B. Zimmermann, H. D. Kjeldsen, M. David-Pur, Y. Hanein, and E. Sernagor, "Carbon nanotube electrodes for retinal implants: A study of structural and functional integration over time," *Biomaterials*, vol. 112, pp. 108–121, Jan. 2017.

[33] R. J. Jensen, J. F. Rizzo, O. R. Ziv, A. Grumet, and J. Wyatt, "Thresholds for activation of rabbit retinal ganglion cells with an ultrafine, extracellular microelectrode," *Investigative Ophthalmol. Vis. Sci.*, vol. 44, no. 8, pp. 3533–3543, Aug. 2003.

[34] C. Sekirnjak *et al.*, "Loss of responses to visual but not electrical stimulation in ganglion cells of rats with severe photoreceptor degeneration," *J. Neurophysiol.*, vol. 102, no. 6, pp. 3260–3269, Dec. 2009.

[35] H. Hashemi, "Distribution of intraocular pressure in healthy Iranian individuals: The Tehran eye study," *Brit. J. Ophthalmol.*, vol. 89, no. 6, pp. 652–657, Jun. 2005.

[36] K. Ren, Y. Zhao, J. Su, D. Ryan, and H. Wu, "Convenient method for modifying poly(dimethylsiloxane) to be airtight and resistive against absorption of small molecules," *Anal. Chem.*, vol. 82, no. 14, pp. 5965–5971, 2010.